Temperature dependence of disorder accumulation and amorphization in Au-ion-irradiated 6*H*-SiC

W. Jiang,* Y. Zhang, and W. J. Weber
Pacific Northwest National Laboratory, P.O. Box 999, Richland, Washington 99352, USA
(Received 8 April 2004; published 25 October 2004)

Disorder accumulation and amorphization in 6*H*-SiC single crystals irradiated with 2.0 MeV Au^{2+} ions at temperatures ranging from 150 to 550 K have been investigated systematically based on 0.94 MeV D^+ channeling analyses along the ⟨0001⟩ axis. Physical models have been applied to fit the experimental data and to interpret the temperature dependence of the disordering processes. Results show that defect-stimulated amorphization in Au^{2+}-irradiated 6*H*-SiC dominates the disordering processes at temperatures below 500 K, while formation of clusters becomes predominant above 500 K. Two distinctive dynamic recovery stages are observed over the temperature range from 150 to 550 K, resulting from the coupled processes of close-pair recombination and interstitial migration and annihilation on both sublattices. These two stages overlap very well with the previously observed thermal recovery stages. Based on the model fits, the critical temperature for amorphization in 6*H*-SiC under the Au^{2+} ion irradiation conditions corresponds to 501 ± 10 K.

DOI: 10.1103/PhysRevB.70.165208 PACS number(s): 61.80.Jh, 61.80.Az, 61.82.Fk, 61.85.+p

I. INTRODUCTION

Over the last decades, considerable efforts have been devoted to the study of radiation effects and defect recovery processes in silicon carbide (SiC). The research has been greatly inspired due to the many outstanding properties (wide band gap, high thermal conductivity and stability, high breakdown electric field strength, high saturated drift velocity, etc.) that make SiC a prominent candidate for high-temperature, high-power and high-frequency microelectronic and optoelectronic devices.[1,2] In addition, SiC has been proposed for structural components in fusion reactors[3] and cladding materials for gas-cooled fission reactors,[4] where high-temperature and high-radiation environments are involved. A fundamental understanding of the disordering behavior in SiC is essential to advance its utilization in these applications.

Since irradiation-induced amorphization processes are both fundamentally and technologically important, various physical models for amorphization in different structures and compositions of ceramic materials have been developed and reviewed.[5] Although these models yield insights into the kinetics of amorphization, very few experimental data are available to determine the parameters for most of the existing models. A simple, useful model for disorder accumulation has been recently proposed to account for the total disorder that consists of the contributions from amorphization, point defects, in-cascade clusters, and extended defect clusters.[6] Experimentally, ion-channeling methods based on Rutherford backscattering spectrometry (RBS/C) or a combination of RBS/C and nuclear reaction analysis (NRA/C) have been frequently employed in the studies to quantitatively determine the degree of disorder in SiC.[5–15] While most of the previous irradiation studies on disorder accumulation in SiC were carried out at or below room temperature, disordering processes in SiC at higher temperatures, which involve significant defect recovery and efficient interstitial precipitation processes during ion irradiation, may be more relevant to semiconductor and nuclear applications. The data for higher temperatures are still largely absent, and the disordering behavior is less understood. This paper reports the dependence of disorder accumulation and dynamic recovery in 6*H*-SiC on irradiation temperature, and an interpretation of the experimental results is given based on model analysis of the data.

II. EXPERIMENTAL PROCEDURES

Irradiation with 2.0 MeV Au^{2+} ions was performed 60° off the surface normal in different areas on ⟨0001⟩-oriented 6*H*-SiC single crystal wafers at various temperatures ranging from 150 to 550 K. A chromel-alumel thermocouple was clamped onto the sample surface for temperature measurements. Ion fluences up to 15 Au^{2+}/nm^2 were applied to produce damage levels from low defect concentrations to the fully amorphous state. Ion fluxes ranged from 0.0038 to 0.0087 $Au^{2+}/nm^2/s$, representing only a small variation at different irradiation temperatures, as given in Table I. Also included in Table I is the local dose rate in displacements per atom per second (dpa/s) at the damage peak. The local dose rate was obtained from the ion flux using a conversion factor $[0.6273\ \text{dpa}/(Au^{2+}/nm^2)]$ calculated from the SRIM97 simulation,[16] where the displacement energy was taken as 20 eV for C and 35 eV for Si sublattice, which are recommended values based on molecular dynamics simulations and experimental results.[17] A combination of 0.94 MeV D^+ $^{28}Si(d,d)^{28}Si$ RBS/C and $^{12}C(d,p)^{13}C$ NRA/C at the scattering angle of 150° was used to simultaneously determine the disorder on both the Si and C sublattices[10] at the depth (116 nm) of the damage peak. The analyzing beam, which was centered in each irradiated area, had an angular dispersion of less than 0.05° and induced negligible damage in the investigated depth region during the channeling analyses. For the Au^{2+} irradiations below room temperature, the irradiated samples were maintained at or below the

 ©2004 The American Physical Society

TABLE I. Experimental conditions used in this study for the Au^{2+} ion irradiation in 6H-SiC.

Temperature (K)	Ion flux ($Au^{2+}/nm^2/s$)	Dose rate (dpa/s)
150	0.0066	0.004 14
170	0.0038	0.002 38
250	0.0043	0.002 70
300	0.0063	0.003 95
370	0.0049	0.003 07
410	0.0050	0.003 14
450	0.0087	0.005 46
500	0.0042	0.002 63
550	0.0087	0.005 46

irradiation temperature during the interim technical procedures for switching from Au^{2+} to D^+ ions and realigning the irradiated crystal to the incident D^+ beam and during *in situ* channeling analysis. For irradiations at or above 300 K, disorder measurements were performed *in situ* at room temperature. These procedures are considered important to minimize the thermal recovery of disorder in the samples prior to the channeling analysis.

III. RESULTS AND DISCUSSION

A. Disorder accumulation

The accumulated disorder at the damage peak (depth =116 nm) for both the Si and C sublattices is shown in Fig. 1 as a function of dose for 6*H*-SiC irradiated at temperatures ranging from 150 to 550 K. The disorder was extracted from the 0.94 MeV D^+ ⟨0001⟩-aligned RBS/C and NRA/C spectra using a linear dechanneling approximation.[11] This simple method is useful to obtain the disorder at the damage peak with comparable precision to an iterative procedure that can extract the depth profile of disorder.[18–20] The solid lines in the figure are data fits using a recent model.[6] In this model, the total disorder, S, produced under ion-beam irradiation and measured by ion-channeling methods is given by the expression[6]

$$S = f_a + S_d + S_c, \tag{1}$$

where f_a and S_d are the contributions from irradiation-induced amorphization and irradiation-induced point defects and in-cascade clusters in the residual crystalline regions, respectively.[21] The third term (S_c) corresponds to the contribution from extended defect clusters or precipitates formed at high temperatures. A related model for disorder accumulation based on a rate-theory expression was proposed by Hecking and co-workers for silicon,[22] but a complete analytical solution is unavailable.

The amorphous fraction, f_a, is well described using a direct-impact/defect-stimulated (DI/DS) model for amorphization:[5]

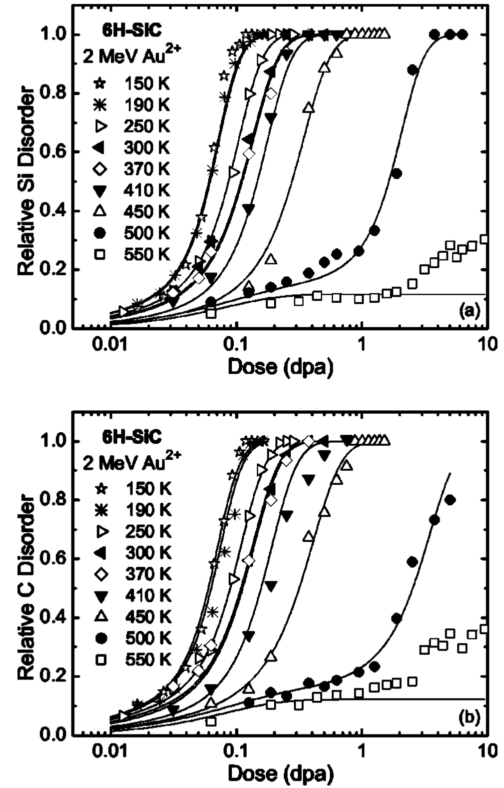

FIG. 1. Relative disorder at the damage peak (depth=116 nm) on (a) the Si and (b) C sublattices as a function of local dose in displacements per atom (dpa) for 6H-SiC irradiated with 2.0 MeV Au^{2+} ions at temperatures ranging from 150 to 550 K. The solid lines are the model fits to the data using Eqs. (1)–(4).

$$f_a = 1 - (\sigma_a + \sigma_s)/\{\sigma_s + \sigma_a \exp[(\sigma_a + \sigma_s)D]\}, \tag{2}$$

where σ_a is the amorphization cross section for the direct-impact process, σ_s is the effective cross section for defect-stimulated amorphization, and D is the local dose. As discussed in detail elsewhere,[5] the DI/DS model [Eq. (2)] provides an analytical solution to the amorphization rate within the Hecking model.[22]

The contribution of irradiation-induced point defects is based on a simple defect accumulation model,[23,24] rather than the Hecking model,[22] and is expressed by the relation[6,21]

$$S_d = S_d^*[1 - \exp(-BD)](1 - f_a), \tag{3}$$

where S_d^* is the saturation value for the defect-induced disorder observed along a specified channel direction, which is proportional to the local displacement rate, and B is proportional to an effective recombination volume for the specific defects giving rise to S_d. As noted previously,[6,21] Eq. (3) is consistent with the observed behavior for the accumulation of point defects in electron-irradiated SiC.[25]

As a first-order approximation, the disorder accumulation due to extended defect clusters S_c has a form similar to the point defect production,[6]

TABLE II. Model parameters from fits of Eqs. (1)–(4) to the experimental data in Fig. 1.

	Si sublattice						C sublattice					
T (K)	σ_a (dpa^{-1})	σ_s (dpa^{-1})	S_d*	B (dpa^{-1})	S_c*	R (dpa^{-1})	σ_a (dpa^{-1})	σ_s (dpa^{-1})	S_d*	B (dpa^{-1})	S_c*	R (dpa^{-1})
150	2.0	51.5	0.045	100	0.0	⋯	2.0	51.5	0.060	100	0.0	⋯
190	2.0	50	0.042	100	0.0	⋯	2.0	48.0	0.055	100	0.0	⋯
250	2.0	30	0.032	100	0.0	⋯	2.0	28.0	0.050	100	0.0	⋯
300	2.0	20.7	0.025	100	0.0	⋯	2.0	20.3	0.040	100	0.0	⋯
370	2.0	20.0	0.020	100	0.0	⋯	2.0	19.5	0.030	100	0.0	⋯
410	1.30	17.0	0.015	100	4×10^{-10}	12	1.30	15.0	0.025	100	5×10^{-10}	12
450	0.80	7.85	0.010	100	0.030	12	0.80	5.95	0.020	100	0.039	12
500	0.08	1.66	0.007	100	0.120	12	0.08	0.78	0.010	100	0.125	12
550	0.0	⋯	7×10^{-4}	100	0.115	12	0.0	⋯	1×10^{-3}	100	0.120	12

$$S_c = S_c^*[1 - \exp(-RD)](1 - f_a), \tag{4}$$

where S_c^* is the saturation value of disorder due to formation of the extended clusters and R is proportional to an effective sink strength to form the extended clusters. A more exact treatment of clustering requires a rate-theory approach, as suggested in the Hecking model,[22] but is beyond the scope of the present investigation.

Based on Eqs. (1)–(4), the fitting parameters for the Si and C data in Figs. 1(a) and 1(b), respectively, are summarized in Table II. The dotted spaces for R at and below 370 K indicate that the S_c term [Eq. (4)] was not included in the data fitting, and those for σ_s at 550 K mean that defect-stimulated amorphization does not play a role since $f_a=0$ when $\sigma_a=0$ [see Eq. (2)]. Parameters B and R are only weakly dependent on irradiation temperature, and the values of B and R, which are the same for the Si and C sublattices, were estimated to be 100 and 12 dpa^{-1}, respectively, over the entire temperature range investigated (150–550 K). While σ_s is slightly sublattice dependent (reflecting the different mobilities of defects on the sublattices in SiC), σ_a is identical for the Si and C sublattices because of the stoichiometric nature of the amorphous state in SiC (i.e., no local enhancement in either element). Some physical constraints were applied during the fitting procedure. For instance, S_d^* decreases with irradiation temperature, while S_c^* contributes to the total disorder only at higher temperatures, where loop formation is observed.

In Fig. 1, there is a similar disordering behavior on the Si and C sublattices in 6*H*-SiC under the irradiation conditions. The accumulation curve shifts to a higher dose with increasing temperature due to a higher rate of simultaneous recovery at higher temperatures. The dose shift is very small between 150 and 190 K and between 300 and 370 K, indicating that two dynamic recovery stages exist over the irradiation temperature range between 190 and 300 K, and above 370 K. The amorphization dose increases from 0.12 dpa at 150 K to 3.76 dpa at 500 K. Complete amorphization does not occur at 550 K for doses up to ~10 dpa, where defect precipitation is a dominant process as will be discussed further below. It is noted that the model fits for both the Si and C sublattices deviate from the experimental data at doses above 1 dpa for the irradiation at 550 K. This could be attributed to several effects. The primary disordering process at this temperature is associated with the formation of stacking faults and dislocation loops during irradiation. Interactions between the interstitial precipitates and the lattice atoms at this temperature can cause a deformation of the local crystal structure, which enhances the backscattering yield. Likewise, the possible formation of vacancy clusters or voids within the crystal structure can also modify the local structure and result in additional lattice displacements. Moreover, a possible change in diffusion efficiency due to the modification of the local structures and compositions of the implanted Au could lead to an alteration of the disordering behavior at the damage peak, since substantial diffusion of the Si (and C) interstitials occurs during Au^{2+} irradiation in 6*H*-SiC at 550 K.[14] In spite of these possible effects that could increase the total disorder, the level of total disorder at the damage peak is relatively low because a great majority of point defects produced during Au^{2+} irradiation are simultaneously recovered at this temperature (550 K).

The fitting results for the Si sublattice at 150, 300, 500, and 550 K are shown in Figs. 2(a)–2(d), respectively, along with the contributions from each of the modeled processes (amorphization, point defects and in-cascade clusters, and precipitates). The results for the C sublattice exhibit similar behavior and thus, are not discussed here. There are several prominent features involved in the disordering processes over this temperature range. At temperatures below 300 K, amorphization processes dominate over nearly the entire range of dose [Figs. 2(a) and 2(b)]. Point defect production at 150 K contributes significantly to the total disorder at low doses below 0.02 dpa. However, the concentration of point defects that survive in the irradiated 6*H*-SiC decreases noticeably at 300 K and effectively vanishes at 550 K. Interstitial precipitation does not play an important role until the irradiation temperature reaches about 500 K, where the Si interstitials also become mobile. At 500 K, nucleation and growth of clusters are the dominant disordering process at doses below 0.3 dpa, and continue to significantly contribute

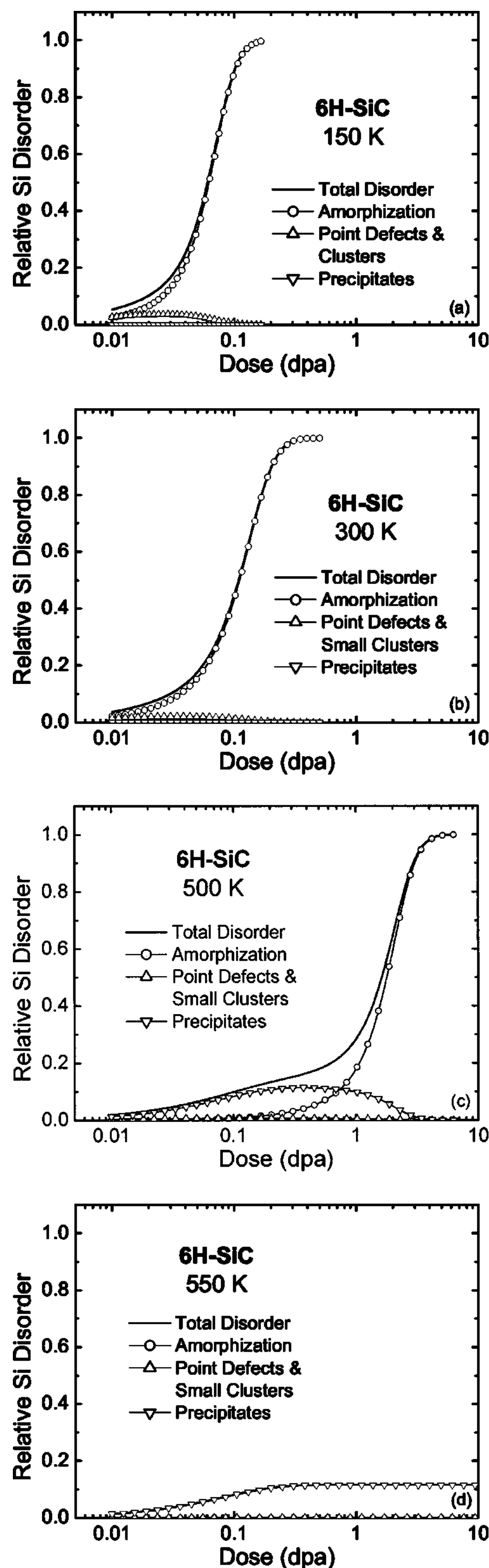

FIG. 2. Model-fitting results for disorder accumulation in 6H-SiC irradiated at (a) 150 K, (b) 300 K, (c) 500 K, and (d) 550 K with corresponding contributions from amorphization, point defects and in-cascade clusters, and extended defect clusters (precipitates) as a function of dose at the damage peak.

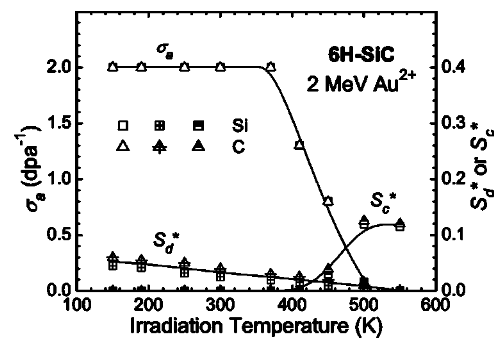

FIG. 3. Model parameters σ_a, S_d^*, and S_c^* as a function of irradiation temperature. The solid lines are drawn for different parameters to guide the eye.

to the total disorder up to doses of about 1 dpa. Amorphization is not active below about 0.1 dpa at 500 K, but dominates the disordering process above 1 dpa [Fig. 2(c)]. Complete amorphization at 550 K does not occur in the Au^{2+} irradiated 6H-SiC, and the predominant disordering process at this temperature is defect precipitation [Fig. 2(d)]. In general, for temperatures at or below 500 K, greater contributions to the total disorder are found for point defects (S_d^*) at low doses, for extended clusters (S_c^*) at low to medium doses, and for amorphization (σ_a and σ_s) at higher doses. As expected, the results are consistent with those for Al^+ irradiated 4H-SiC over a similar temperature range.[6]

Figure 3 shows the temperature dependence of the amorphization cross section (σ_a) and the saturation values for defect-induced disorder (S_d^*) and for precipitated clusters (S_c^*) in Au^{2+} irradiated 6H-SiC observed along the $\langle 0001 \rangle$ axis. Because of the shadowing effects from the $\langle 0001 \rangle$ atomic strings in 6H-SiC,[11] the S_d^* value will be greater, particularly for the C sublattice, when viewed along other off-axes for the channeling measurements. From Fig. 3 and Table II, the parameter, σ_a, for both the Si and C sublattices remains constant at 2.0 dpa^{-1} between 150 and 370 K, above which the σ_a value decreases with increasing temperature and vanishes at ~500 K. The constant value of σ_a in the low temperature range indicates that the amorphization process due to direct impact of Au^{2+} ions onto 6H-SiC crystals is not significantly affected by thermal processes during ion irradiation at the low temperatures. Between 370 and 500 K, however, more thermal processes become active, which decrease the amount of direct-impact amorphization. With the increase of temperature in this range, a larger amount of amorphization from the direct-impact process is prohibited due to the increasing rate of competitive recovery processes, resulting in a monotonic decrease in the σ_a value. For lighter-ion irradiations that produce a lower damage energy density, the amorphization cross section, σ_a, is expected to start decreasing at lower temperatures. Again from Fig. 3, the fitting parameter, S_d^*, decreases linearly with irradiation temperature, and S_c^* becomes a nonzero value at 450 K and increases to ~0.12 at 500 and 550 K. The decrease in the production rate of stable point defects with increasing temperature is primarily attributed to more probable recombination events for close pairs and the annihilation of mobile interstitials at sinks. In general, interstitial migration and ag-

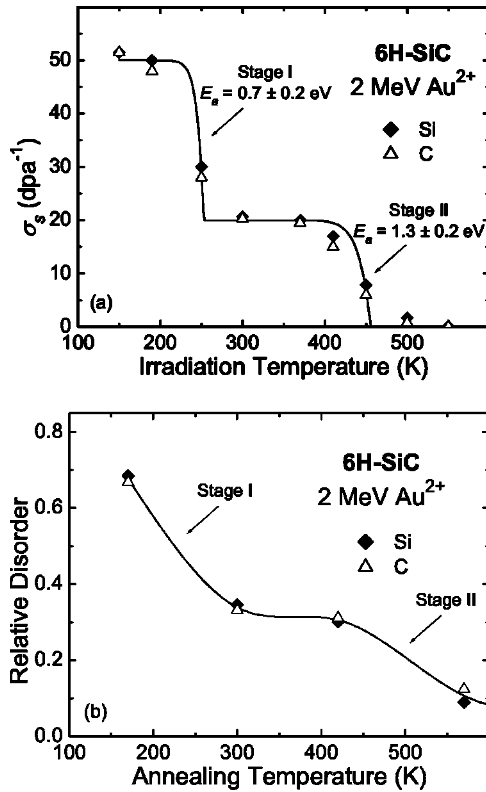

FIG. 4. (a) Effective cross section for defect-stimulated amorphization (σ_s) as a function of irradiation temperature. The solid line is the model fit from Eq. (6); (b) isochronal recovery (20 min) of relative disorder on the Si and C sublattices in Au^{2+}-irradiated 6H-SiC as a function of annealing temperature. The solid line is drawn to guide the eye.

gregation produce extended defect clusters, and elevated temperatures expedite the precipitation process. It is expected that the size of the precipitates increases with increasing ion fluence and irradiation temperature.

B. Dynamic recovery

Also of interest is the dynamic recovery during ion irradiation, since this process controls the temperature-dependent behavior during irradiation. Of the model parameters used to fit the temperature dependent data, σ_s is the primary parameter controlling amorphization. The values of σ_s are shown in Fig. 4(a) as a function of temperature for both the Si and C sublattices, and the results indicate two well-defined stages of decreasing σ_s that are due to dynamic recovery processes. There is no significant difference in the behavior for Si and C, which is expected since amorphization is largely a stoichiometric process. The dynamic recovery stages represented in Fig. 4(a) are similar to thermal recovery stages previously observed during isochronal annealing of 6H-SiC irradiated with 2 MeV Au^{2+},[26] as shown in Fig. 4(b). While the incremental temperature steps are larger in the prior thermal annealing study, there is a clear correlation between the dynamic and thermal recovery stages. In contrast, 4H-SiC irradiated with Al^{+} ions exhibits rather continuous dynamic recovery between 150 and 450 K;[6] however, the results in the present study are consistent with the thermal annealing observed in 4H-SiC over the same temperature range.[21]

TABLE III. Activation energies (eV) measured for dynamic recovery in 6H-SiC in this study and predicted from molecular dynamics simulations in 3C-SiC (Refs. 27 and 29).

	Dynamic recovery	C close pairs	Si close pairs	Interstitial migration
Stage I	0.7±0.2		0.9 (Si_{TC})	0.74 (C)
Stage II	1.3±0.2	1.3 (C–Si ⟨110⟩) 1.6 (C_{TS})		1.53 (Si)

Simultaneous recovery of the defects produced during ion irradiation may occur due to close-pair recombination and long-range migration of point defects that result in recombination or annihilation of the point defects in the crystalline state and point defect annihilation or epitaxial recrystallization at crystalline–amorphous interface. The recovery can be due to thermal or irradiation-enhanced processes. The recovery rate, $K(T)$, for the irradiation enhanced or thermal annealing process at temperature, T, can be expressed by[5]

$$K(T) = \nu \exp(-E_a/kT), \tag{5}$$

where ν is the effective attempt frequency, E_a is the activation energy for an irradiation-assisted or thermal recovery process, and k is the Boltzmann constant. The effective cross section for defect-stimulated amorphization, σ_s, is dependent on $K(T)$, and the temperature dependence of σ_s is given by the expression:[5]

$$\sigma_s = \sigma_{s0} - K(T)/\phi = \sigma_{s0} - (\nu/\phi)\exp(-E_a/kT), \tag{6}$$

where the quantities ϕ and σ_{s0} are the dose rate (dpa/s) and effective cross section (dpa^{-1}) for defect-stimulated amorphization at $T=0$ K, respectively. Based on recent molecular dynamics (MD) simulations,[27] the value of ν for close-pair recombination in SiC ranges from 3×10^{12} to 5×10^{14} s^{-1}. Since most dynamic recovery will occur within the cascades, a value of $\nu=10^{13}$ s^{-1} is assumed for the data fitting. Under the experimental conditions of this study (Table I), the average damage rate is about 3×10^{-3} dpa/s. Using these values for ν and ϕ, Eq. (6) has been fit to the results in Fig. 4(a), as indicated by the solid curve. The values for σ_{s0} are determined to be 50 and 20 dpa^{-1}, and the activation energies, which are summarized in Table III, are 0.7±0.2 and 1.3±0.2 eV for the first and second dynamic recovery stages, respectively. The errors on the activation energies are associated with uncertainties in the absolute temperatures and in the value for ν. The activation energy of 1.3±0.2 eV for the second stage dynamic recovery is in excellent agreement with the value of 1.3 eV determined for dynamic annealing in 4H-SiC by Kuznetsov *et al.*[28] This value is higher than the value of 0.9 eV estimated for the activation energy from the critical temperature for amorphization in 4H-SiC,[12] but that study assumed $\nu=10^{9}$ s^{-1}. If one assumes the same value of ν as in the present study, the results from that study yield an activation energy of 1.25 eV in agreement with the results

here and those of Kuznetsov *et al.*[28] While none of these studies provided rigorous determinations of activation energies, the results based on the different methodologies are similar and suggest that the activation energy for the recovery process that inhibits amorphization in SiC appears to be on the order of 1.3 eV.

Since the near-neighbor environments in the 6H and 3C polytypes are the same, the activation energies for close-pair recombination in 3C-SiC determined by MD simulations[27] are relevant to the present study. The MD simulations indicate that the activation energies for close-pair recombination in 3C-SiC are mostly in the range of 0.23–0.38 eV, which are below those estimated here. However, the activation energy for recombination of the Si tetrahedral interstitial (Si_{TC}) surrounded by four C atoms is 0.9 eV (Table III),[27] which is in reasonable agreement with the activation energy determined for the first dynamic stage. The C–Si ⟨110⟩ split interstitial on a Si site and the C tetrahedral interstitial (C_{TS}) surrounded by four Si atoms have activation energies for close-pair recombination (Table III) of 1.3 and 1.6 eV, respectively,[27] which are also consistent with the activation energy estimated for the second dynamic recovery stage. Furthermore, recent MD simulations[29] of intrinsic defect migration in 3C-SiC indicate that long-range interstitial migration energies are 0.74 and 1.53 eV for C and Si interstitials, respectively, as indicated in Table III, which are consistent with the activation energies determined in the present study. The results in Table III suggest that both Si and C close-pair recombination and in-cascade short-range migration of C and Si interstitials may be responsible for the dynamic recovery stages. This interpretation is also consistent with the coupled recovery observed on both the C and Si sublattices during thermal recovery, as shown in Fig. 4(b).

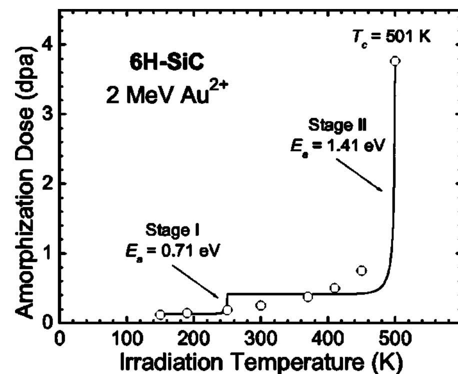

FIG. 5. Temperature dependence of dose for full amorphization in 6H-SiC under the Au^{2+} ion irradiation. The solid lines are the model fits to the data using Eq. (8).

C. Amorphization

The dose required for full amorphization (amorphization dose) in 6H-SiC under the Au^{2+} irradiation conditions is illustrated in Fig. 5 as a function of irradiation temperature. The data points in the figure are taken from the experimental results shown in Fig. 1 and have an uncertainty of ~10%. Obviously, amorphization occurs only if the rate of amorphization or disordering is greater than the rate of simultaneous recovery during irradiation. An expression from the kinetic DI/DS model for amorphization has been derived,[5] which has the form:

$$D = (D_0 + A\phi \ln\{1 - AK(T) \times [1 - \exp(-D_0/A\phi)]\})/[1 - AK(T)], \quad (7)$$

where $A=[\phi(\sigma_a+\sigma_s)]^{-1}$. By inserting Eq. (5) into Eq. (7), Eq. (7) becomes

$$D = \frac{D_0 + \frac{1}{(\sigma_a+\sigma_s)}\ln\left\{1 - \frac{\nu}{\phi\times(\sigma_a+\sigma_s)}\exp\left(-\frac{E_a}{kT}\right)\times[1-\exp[-D_0\times(\sigma_a+\sigma_s)]]\right\}}{1 - \frac{\nu}{\phi\times(\sigma_a+\sigma_s)}\exp\left(-\frac{E_a}{kT}\right)}. \quad (8)$$

The result from the data fit using Eq. (8) is shown in Fig. 5 over the two temperature ranges, corresponding to the disorder recovery stages [Fig. 4(a)]. In the data fitting, the effective jump frequency and dose rate were chosen as $\nu = 10^{13}\ s^{-1}$ and $\phi = 3\times10^{-3}$ dpa/s, respectively. These are the same values as those adopted for fitting the data in Fig. 4(a). From Table II, the sum of the amorphization cross sections for direct impact and defect-stimulated processes $(\sigma_a+\sigma_s)$ is equal to 52 and 22 dpa^{-1} in the first and second dynamic recovery processes, respectively. As a result of the model fits, the activation energy for the two stages corresponds to $E_a(I)=0.71$ eV and $E_a(II)=1.41$ eV with $D_0(I)=0.13$ dpa and $D_0(II)=0.41$ dpa, respectively. The resulting values of activation energy agree well with those for the corresponding dynamic recovery stages (Table III). Note that the data fits in both Figs. 4(a) and 5 are not perfect, particularly for stage II. This is due to irradiation-assisted recovery processes that provide an additional low-level of recovery over the temperature range of each stage, as described elsewhere,[5] as well as to a range of dynamic recovery processes with different activation energies and jump frequencies. The latter interpretation is supported by the MD simulation results (Table III)[27,29] that suggest comparable activation energies for Si (C) close-pair recombination and C (Si) interstitial migration

and annihilation at stage I (II). In addition, experimental error ($\sim 10\%$) for the amorphization dose in Fig. 5 may also contribute to the deviation of the model fit from the data points.

As the irradiation temperature approaches to 500 K, the rate of simultaneous recovery increases exponentially [Fig. 4(a)]. This leads to a slower rate of disorder accumulation and a higher dose is required to achieve the same level of disorder. At the critical temperature, T_c, for amorphization, complete amorphization does not occur due to the perfect balance of disorder production and recovery. In this case, the amorphization dose, D, approaches infinity at T_c. According to Eq. (8):

$$1 - \frac{\nu}{\phi \times (\sigma_a + \sigma_s)} \exp\left(\frac{-E_a}{kT}\right) = 0 \text{ at } T = T_c.$$

Thus,

$$T_c = E_a/(k \ln\{\nu/[(\sigma_a + \sigma_s)\phi]\}), \tag{9}$$

where E_a corresponds to the activation energy for the second recovery process (E_a=1.41 eV). Numerical evaluation results in a value of T_c=501 K for 6H-SiC under the Au^{2+} irradiation conditions. This value, which has an uncertainty of ± 10 K, should be viewed as an estimate only. This is because only a single thermal recovery process was used in fitting. More accurate determination of T_c requires more data points and a more rigorous model that includes irradiation-assisted processes. However, from Figs. 1 and 5, it appears that the critical temperature for amorphization under the irradiation conditions of this study is close to 500 K. While this critical temperature for SiC under 2 MeV Au^{2+} irradiation is higher than values for electrons (295 K)[30] or lighter ions, such as Ne^{+} (421 K),[9] Al^{+} (450 K),[6] and Xe^{+} (485 K),[9] it is consistent with the systematic increase in critical temperature with damage energy density (ion mass) observed previously for 6H-SiC.[8,9] For larger masses, a higher damage energy density is produced, leading to the formation of more complex defects that affect the dynamic annealing behavior. A more detailed discussion about the effects of ion mass on the critical temperature for amorphization has been provided previously.[5,9]

IV. CONCLUSIONS

It has been shown that the disordering behavior on the Si and C sublattices in Au^{2+} irradiated 6H-SiC is similar at temperatures ranging from 150 to 550 K. Model fits indicate that amorphization in 6H-SiC under Au^{2+} ion irradiation at temperatures below 500 K is a dominant process. Generation of point defects and in-cascade clusters that survive at low temperatures (150 K) contribute significantly to the total disorder below 0.02 dpa. At 500 K, precipitation processes become dominant in 6H-SiC below 0.3 dpa, while amorphization governs the disordering process above 1 dpa. Nucleation and growth of clusters is nearly the only active process at 550 K and above. Two dynamic recovery stages are observed with activation energies of 0.7 ± 0.2 eV and 1.3 ± 0.2 eV, respectively. In addition, model fits for the amorphization dose yield similar activation energies (0.71 and 1.41 eV) for the two corresponding stages. The critical temperature for amorphization is estimated to be 501 ± 10 K for 6H-SiC under the Au^{2+} irradiation conditions.

ACKNOWLEDGMENTS

This research was supported by the Division of Materials Sciences and Engineering, Office of Basic Energy Sciences, U.S. Department of Energy. Support for the accelerator facilities within the Environmental Molecular Sciences Laboratory (EMSL) was provided by the Office of Biological and Environmental Research, U.S. Department of Energy. The Pacific Northwest National Laboratory is operated by Battelle Memorial Institute for the U.S. Department of Energy under Contract No. DE-AC 06-76RLO 1830.

*Author to whom correspondence should be addressed: Pacific Northwest National Laboratory, MSIN K8-93, P.O. Box 999, Richland, WA 99352; electronic address: weilin.jiang@pnl.gov

[1] *Proceedings of the International Conference on SiC and Related Materials*, edited by R. F. Davis (IOP, London, 1994).

[2] C. Raynaud, J. Non-Cryst. Solids **280**, 1 (2001).

[3] P. Fenici, A. J. Frias Rebelo, R. H. Jones, A. Kohyama, and L. L. Snead, J. Nucl. Mater. **258–263**, 215 (1998).

[4] B. G. Kim, Y. Choi, J. W. Lee, Y. W. Lee, D. S. Sohn, and G. M. Kim, J. Nucl. Mater. **281**, 163 (2000).

[5] W. J. Weber, Nucl. Instrum. Methods Phys. Res. B **166–167**, 98 (2000).

[6] Y. Zhang, W. J. Weber, W. Jiang, C. M. Wang, V. Shutthanandan, and A. Hallén, J. Appl. Phys. **95**, 4012 (2004).

[7] C. J. McHargue and J. M. Williams, Nucl. Instrum. Methods Phys. Res. B **80–81**, 889 (1993).

[8] E. Wendler, A. Heft, and W. Wesch, Nucl. Instrum. Methods Phys. Res. B **141**, 105 (1998).

[9] W. J. Weber, N. Yu, L. M. Wang, and N. J. Hess, Mater. Sci. Eng., A **253**, 62 (1998).

[10] W. Jiang, W. J. Weber, S. Thevuthasan, and R. Grötzschel, Nucl. Instrum. Methods Phys. Res. B **161–163**, 501 (2000).

[11] W. Jiang and W. J. Weber, Phys. Rev. B **64**, 125206 (2001).

[12] Y. Zhang, W. J. Weber, W. Jiang, C. M. Wang, A. Hallén, and G. Possnert, J. Appl. Phys. **93**, 1954 (2003).

[13] W. Jiang and W. J. Weber, *Recent Research and Development in Applied Physics*, edited by S. G. Pandalai (Transworld Research Network, Kerala, India, 2003), Vol. 6, p. 415.

[14] W. Jiang, W. J. Weber, Y. Zhang, S. Thevuthasan, and V. Shuttanandan, Nucl. Instrum. Methods Phys. Res. B **207**, 92 (2003).

[15] W. J. Weber, N. Yu, L. M. Wang, and N. J. Hess, J. Nucl. Mater. **244**, 258 (1997).

[16] J. F. Ziegler, J. P. Biearsack, and U. Littmark, in *The Stopping*

and Range of Ions in Solids (Pergamon, New York, 1985); available from: http://www.SRIM.org/.

[17] R. Devanathan, W. J. Weber, and F. Gao, J. Appl. Phys. **90**, 2303 (2001).

[18] J. S. Williams and R. G. Elliman, in *Ion Beams for Materials Analysis*, edited by J. R. Bird and J. S. Williams (Academic, San Diego, 1989), p. 286.

[19] M. L. Swanson, in *Handbook of Modern Ion Beam Materials Analysis*, edited by J. R. Tesmer and M. Nastasi (Materials Research Society, Pittsburgh, PA, 1995), p. 267.

[20] W. Jiang, W. J. Weber, C. M. Wang, L. M. Wang, and K. Sun, Defect Diffus. Forum **226–228**, 91 (2004).

[21] Y. Zhang, W. J. Weber, W. Jiang, A. Hallén, and G. Possnert, J. Appl. Phys. **91**, 6388 (2002).

[22] N. Hecking, K. F. Heidemann, and E. te. Kaat, Nucl. Instrum. Methods Phys. Res. B **15**, 760 (1986).

[23] F. L. Vook and H. J. Stein, Radiat. Eff. **2**, 23 (1969).

[24] W. J. Weber, J. Nucl. Mater. **98**, 206 (1981).

[25] A. Matsunaga, C. Kinoshita, K. Nakai, and Y. Tomokiyo, J. Nucl. Mater. **179–181**, 457 (1991).

[26] W. Jiang, W. J. Weber, S. Thevuthasan, and V. Shuttanandan, J. Nucl. Mater. **289**, 96 (2001).

[27] F. Gao and W. J. Weber, J. Appl. Phys. **94**, 4348 (2003).

[28] A. Yu. Kuznetsov, J. Wong-Leung, A. Hallén, C. Jagadish, and B. G. Svensson, J. Appl. Phys. **94**, 7112 (2003).

[29] F. Gao, W. J. Weber, M. Posselt, and V. Belko, Phys. Rev. B **69**, 245205 (2004).

[30] H. Inui, H. Mori, and H. Fujita, Philos. Mag. B **61**, 107 (1990).